Title

Strongly Correlated Aromatic Molecular Conductor

Journal

Small, 15(14)

ISSN

1613-6810

Authors

Hu, Yong

Zhong, Guohua

Guan, Ying-Shi

et al.

Publication Date

2019-04-01

DOI

10.1002/smll.201900299

Peer reviewed

Strongly Correlated Aromatic Molecular Conductor

Yong Hu, *Guohua Zhong*, *Ying-Shi Guan*, *Jason N. Armstrong*, *Changning Li*, *Changjiang Liu*,

Alpha N'Diaye, *Anand Bhattacharya*, *and Shenqiang Ren**

Y. Hu, Dr. Y.-S Guan, Dr. J. N. Armstrong, C. N. Li, Prof. S. Q. Ren

Department of Mechanical and Aerospace Engineering, Research and Education in Energy, Environment & Water (RENEW) Institute

University at Buffalo

The State University of

New York Buffalo, New

York 14260, USA E-mail:

shenren@buffalo.edu

Prof. G. H. Zhong

Shenzhen Institutes of Advanced

Technology Chinese Academy of

Sciences

Shenzhen 518055, China

Dr. C. J. Liu, Prof. A.

Bhattacharya Materials

Science Division Argonne

National Laboratory

Lemont, IL 60439, USA

Prof. A. N'Diaye

Lawrence Berkeley National

Laboratory Berkeley, CA 94720.

Prof. A. Bhattacharya

Center for Nanoscale

Materials Argonne

National Laboratory

Lemont, IL 60439, USA

Keywords: charge-transfer, molecular conductor, aromatic molecule, surface plasmon resonance

Abstract

Strongly correlated electronic molecules open the way for strong coupling between charge, spin, and lattice degrees of freedom to enable interdisciplinary fields, such as molecular electronic switches and plasmonics, spintronics, information storage, and superconducting circuits. However, despite exciting computational predictions and promising advantages to prepare flexible geometries, electron correlation effect in molecules has been elusive. Here we report the electron correlation effects of molecular plasmonic films to uncover its coupling of charge, spin, lattice, and orbital for switchable metal-to-insulator transition under external stimuli, at which the simultaneous transition occurs from paramagnetic, electrical and thermal conducting state to diamagnetic, electrical and thermal insulating state. In addition, we combine density functional theory calculation and spectroscopic studies to provide the mechanistic understanding of electronic transitions and molecular plasmon

resonance observed in molecular conducting films. The self-assembled molecular correlated conductor paves the way for the next generation integrated micro/nanosystems.

Introduction

Materials in which the electrons are strongly correlated show unusual electronic, optical, and magnetic properties, including metal-insulator transition (MIT),[1] colossal magnetoresistance[2] and high-temperature

superconductivity.[3] The manipulation and use of

these correlated phenomena enable the applications in smart windows, magnetic storage technologies and superconducting magnets.[4-6] An important characteristic of these materials is the existence of several competing states which simultaneously involves different physical channels, showing the possibility to tune the correlated properties with external field. Among them, the strongly correlated electronic inorganic materials, such as VO_2,[7] MoS_2,[8, 9] and $Pr_{0.7}Ca_{0.3}MnO_3$,[10] have attracted considerable attention due to the simultaneous physical properties change accompanied at MIT. However, despite exciting theoretical predictions and promising advantages to prepare flexible geometries, the correlated electronic molecules have rarely been studied.[11],[12] Thus, exploring electron correlation in molecules with the coupling between charge, spin, and lattice degrees of freedom is urgent for a change of paradigm in polarotonics that hold great potential for molecular electronics.

Among the reported strongly correlated electronic molecules, alkali-metal-intercalated aromatic hydrocarbons show promising as a candidate to show the strong coupling between charge, spin and lattice degrees of freedom for the advancement of molecular electronics and plasmonics. However, its bulk form with abundant defects usually makes it challenging to probe its intrinsic physical properties.[13] For example, bulk systems with disordered structure do not usually exhibit metallic conduction even with a high carrier concentration and high conductivity at room temperature, due to the disorder-induced localization of carriers at lower temperature, namely Fermi-glass characteristics.[14] One intriguing way to overcome this

difficulty is to fabricate molecular thin films with a size smaller than the characteristic domain size, which can considerably reduce the grain boundary defects. Here we report the electron correlation in molecular plasmonic conducting films, potassium intercalated p-terphenyl $K_3C_{18}H_{14}$ (k-TP). The pristine p-terphenyl is an intrinsic semiconductor with the wide bandgap of 3.37 eV. Upon alkali-metal doping, we find that the p-terphenyl gives rise to a metallicity and surface plasmon resonance in an otherwise insulating solid at room-

temperature. The coupling of lattice, charge, spin, and orbital in the k-TP films enables unusual electrical, thermal, and magnetic transitions around the MIT, at which the simultaneous transition occurs from paramagnetic, electrical and thermal conducting state to diamagnetic, electrical and thermal insulating state. The switchable MIT of k-TP can be tuned across a broad range through the control of the intercalation. In addition, the k-TP thin film shows a distinct change in its electrical conductivity under external stimuli in the MIT region. The density functional theory and spectroscopic studies provide the mechanistic understanding of electronic correction and transitions, as well as surface plasmonic resonance in molecular conducting films.

Results

Charge transfer has been proved to be an efficient way to induce metallic conductivity in an insulating organic molecule, where charge carriers are stabilized by the existence of counter ions so as to maintain their charge neutrality, and they provide strong intermolecular interaction, which delocalizes conducting electrons.[15] More interestingly, the obtained charge transfer complexes usually show a MIT due to the interaction between electrons. Based on the thermal stability of p-terphenyl (Figure S1), we grow the charge transfer complex k-TP thin films in a sealed glass tube under high vacuum at 573 K (**Figure 1**a). Scanning electron microscope image in Figure 1b shows a uniform surface from the as-grown k-TP film. The optical image (Inset of Figure 1b) of k-TP thin film shows a

lustrous metallic golden color, suggesting its potential metallic conductivity and distinct optical properties. Inset of Figure S2 shows the atomic force microscope image of a k-TP thin film, confirming the formation of dense and homogeneous surface morphology with thickness of about 50 nm. Raman spectra (Figure 1c) for the pristine p-terphenyl and k-TP thin films indicate the potassium intercalation into p-terphenyl for the formation of a charge-transfer complex. In

addition, the thin film shows the pronounced photoabsorption peaks at 503 nm, 543 nm and

563 nm (Figure S3), indicating the formation of polarons which induce two localized electronic levels in the gap: a singly occupied bonding state above the valence band edge and an empty antibonding state below the conduction-band[16]. More interestingly, the k-TP thin film shows a free-carrier absorption with a remarkably well-defined peak in the near-infrared (NIR) region from polarons (Figure 1d).[17, 18] The NIR absorption may have several resources such as surface plasmon resonance, scattering or sample impurities.[17] The NIR spectra are measured in three different environments: nitrogen atmosphere, hexane, and silicone oil with the refractive indices of 1.00, 1.37, and 1.41, respectively. As shown in inset of Figure 1d, the NIR absorption band redshifts with increasing refractive index, suggesting its origin from surface plasmon resonance of molecular k-TP films.[19] The surface plasmon resonance at room-temperature indicates high density of charge carriers in k-TP thin film.

The temperature dependence of electrical resistivity in k-TP thin films through the four probe method confirms metallic conductivity at room-temperature with an electrical resistivity of 0.08 ohm.cm (**Figure 2**a). Figure 2b shows the current-voltage (I-V) characteristics of the k-TP thin films, which confirms the metallic behaviors in k-TP thin films at room temperature. Upon cooling, the electrical resistivity increase slowly and then freezes into a Mott insulating state, where four orders of magnitude increase in resistivity is observed at 126 K. Inset of Figure 2a shows the logarithm of electrical resistivity/temperature vs. the inverse temperature

for k-TP thin film. It is clearly shown that the slop increase a lot in the MIT temperature range, indicating an increased activation energy. While the k-TP thin film shows a MIT at low temperature, we further explore the possibility to tune its transition temperature. The intercalation of potassium into p-terphenyl plays an important role in the electrical properties through controlling the intermolecular interaction. Here, we modify the intercalation level through two different methods, including the sintering temperature and the

doping ratio of potassium. Based on the thermal stability of p-terphenyl, we carry out the reaction at 543 K and 603 K for the formation of k-TP thin films. Figures S4a and S4b show the temperature dependence of electrical resistivity in k-TP thin films prepared at 543 K and 603 K, respectively. The electrical resistivity for thin films confirms room-temperature metallic conductivity and a low-temperature MIT. The sintering temperature dependence of MIT temperature is presented in Figure S4c (obtained from the temperature dependence of electrical resistivity curves). As shown, slightly increasing or decreasing the reaction temperature can shift the MIT temperature, suggesting that the MIT is sensitive to the reaction temperature. As shown in Figure S4a, at low sintering temperature of 543 K, the obtained k- TP thin film shows higher electrical resistivity of 0.61 ohm-cm and higher MIT temperature of 174 K. The increase in electrical resistivity might result from the low intercalation level due to the low reaction temperature. As for the high reaction temperature of 603 K, a higher electrical resistivity of 1.05 ohm-cm and higher MIT temperature of 206 K are also induced. This might come from the chemical bond formation between potassium and p-terphenyl at high reaction temperature. To support this assumption, X-ray absorption spectroscopy (XAS) was performed with the k-TP prepared at 603 K. As shown in Figure S5, the XAS shows the absorption peak for potassium-carbon bond, indicating the chemical bond formation, which cause the decrease in the electrical conductivity. We further study the effect of intercalation ratio on the MIT temperature of k-TP thin film. Figures S4d and S4e show the temperature dependence of electrical resistivity of $K_2C_{18}H_{14}$ and $K_4C_{18}H_{14}$, respectively.

At 300 K, the measured resistivity is 1.30 ohm-cm and 0.88 ohm-cm for $K_2C_{18}H_{14}$, $K_4C_{18}H_{14}$ thin film, respectively, which are both higher than the electrical resistivity of k-TP thin film. In addition, increasing or decreasing the potassium intercalation can shift the MIT temperature, as shown in Figure S4f which is obtained from the temperature dependence of electrical condutivity curves. To study the carrier-generation mechanism that leads to metallic conduction, we study

magnetic spin coupling of thin films at different doping contents using electron paramagnetic

resonance (EPR). As shown in Figure 2d, the EPR signal enhances with increasing the doping level. It should be mentioned that $K_3C_{18}H_{14}$ shows a wider peak-to-valley linewidth, indicating the EPR happed in a broader magnetic field range. The mechanism for this dopant concentration dependence of electrical conductivity should come from different reason since the lower doping ratio with less polaron and higher doping ratio with more polaron both show decreased electrical conductivity. Our scanning tunneling microscopy study shows that potassium intercalated p-terphenyl forms the dipole molecule which induces one-dimensional molecular chains that extend to a percolating network for electron transport.[20] Therefore, for $K_2C_{18}H_{14}$ thin film, the low doping ratio might reduce the dipole molecule and make it challenging to form conducting molecular chains. The increased electrical resistivity for $K_4C_{18}H_{14}$ thin film arise from other mechanism. As the doping ratio increases, the free electrons are also increased and the unfilled conducting band have a tendency to be filled with more generated free electrons and lower its electrical conductivity.[19]

We further study the structure and dynamics of polarons that contribute to the metallic conductivity of k-TP thin films. Pristine p-terphenyl shows several Raman active modes, including stretching, bending (in-plane deformation), rocking (out-of-plane deformation).[21]-[22] The C-H stretching region, which can be significantly affected by the intermolecular interaction,[23] is the strong feature in the Raman spectra. As shown in Figure 2c, after potassium intercalation into p-terphenyl, the modes in the C-H stretching region shift to the lower frequency. Our

scanning tunneling microscope shows that when potassium is intercalated into p-terphenyl molecule, the k-TP molecule loses its symmetry and becomes a dipole.[20] The dipolar interactions between the potassium intercalated p-terphenyl molecules would affect the C-H frequencies. Theoretical calculation for the influence of intercalation to the C-H length is presented in Figure S6. It is shown that the stretched C-H bond length is resulted from the dipolar interactions between the potassium intercalated p-terphenyl

molecules, which provide the lattice evidence to the change in C-H stretching frequency. The temperature dependence of Raman spectra for k-TP thin films shows that C-H stretching peaks overlap across the full temperature range (Figure S7), indicating the temperature independent dipolar interactions between the potassium intercalated p-terphenyl molecules. In other words, the dipolar interactions between the potassium intercalated p-terphenyl is not the origin for the MIT in k-TP thin films. Thus, we further study the evolution of the distribution of charge on the lattice of these systems around the MIT. The charge distribution is probed by measuring the frequency of the central C-C molecular bond vibration, which changes by about 50 cm^{-1} after cooling form 300 K to 120 K (Figure 2c).[24] This is a result of a lengthening of the central C-C bond of the molecule, in which the charge occupies the highest occupied molecular orbital as shown in the theoretical calculation (Figure S6). As shown in Figure 2d, the EPR signal appears after the potassium intercalation and the signal is enhanced by increasing the intercalation level. The EPR measurements confirm that the radical, the polaron with ½ spin number, emerges after the potassium intercalated into p-terphenyl and acts as the charge carriers.

Theoretical calculation is performed to further understand the intercalation induced metallic conductivity in k-TP. By the first-principles calculations, we predicted the crystal structure of k-TP at ambient pressure, showing the unit cell of k-TP in **Figure 3**a. The lattice parameters are a=14.502 Å, b=5.462 Å, c=10.243 Å, and β =76.13^{0}, respectively. Figure 3b shows the charge transfer from the calculated three-dimensional

plot of different charge density for k-TP. The yellow electron cloud represents the transferred charge from potassium atoms to p- terphenyl molecules. From Figure 3b, we can identify the location of the transferred charge and observe the charge ordering in molecule. Figure 3c shows the calculated band structures along high-symmetry k-path in the first Brillouin Zone where zero energy denotes the Fermi level. It should be noted that the doping results in the Fermi level rising, in k-TP, #1 and #2

bands are fully occupied by electrons, beyond them (#1 and #2), the Fermi level crosses two bands with higher energy, exhibiting metallic behavior. Figure 3d shows the calculated total and projected density of states (DOS/PDOS) of k-TP where zero energy denotes the Fermi level. Analyzing the scale in Figure 3d, we can conclude that the electronic states at Fermi level mainly result from C-p electrons, however, K-s and K-d slightly contribute to the Fermi surface. Additionally, the PDOS showed in Figure 3d indicates the charge transfer from potassium to molecules.

The k-TP films show strong coupling between charge, spin, and lattice degrees of freedom. The strongly coupled electron and lattice degrees of freedom in k-TP films introduce a thermal conductivity change around the MIT region. As shown in **Figure 4**a, an increase in thermal conductivity appears at MIT due to the coupling between charge and lattice degrees of freedom, where the thermal conductivity increases by 14% in the metallic phase. In this case, the k-TP behaves effectively as a thermal switch, as it drastically changes the total thermal conductivity over a narrow temperature range. To study the coupling between charge and spin, the temperature dependence of magnetic susceptibility (χ) of k-TP thin film from 126 K to 300 K is measured (Figure 4b). As the sample is cooled from room temperature, χ of k-TP thin films shows a slight decrease. In the MIT region, the magnetization reduces significantly with the completely quenched paramagnetism, exhibiting a spin-Peierls-like magnetic transition in which one-dimensional paramagnetic spin (S= 1/2) states are converted to the dimerized diamagnetic state at low temperature.[25, 26] The assumption of dimerized diamagnetic states is supported by our

scanning tunneling microscopy study, showing that the potassium intercalated p-terphenyl molecule are paired at low temperature. The sharp decrease in χ shows the similar tendency as electrical conductivity, further suggesting that the polarons with ½ spin number as charger carrier for metallic conductivity. The magnetic measurement indicates a magnetic phase transition coupled with MIT transition, confirming

the coupling between charge and spin degrees of freedom. The magnetic field dependence of electrical properties is also investigated at different electrical states. As shown in Figure 4c, in the metallic state at 300 K, the resistivity for k-TP thin film decreases lineally with increasing magnetic field and reaches up to a negative magnetoresistance of -0.31 % at 4,000 Oe. The negative magnetoresistance effect originates from a suppressed spin scattering, resulting from a spin alignment of polaron with the applied field where the magnetoresistance is decreased lineally with external field up to a large field[27]. In the insulating state at 126 K, k-TP thin film does not show the distinct magnetoresistance due to the diamagnetic property. In contrast, at the MIT region, the k-TP thin film shows an optimum magnetoresistance -0.55 % at 4000 Oe and tend to saturate at this field. Such dramatic magnetoresistance effect in k-TP thin film is resulted from the polaron transition to a triplet bipolaron under external magnetic field in the MIT transition region.

The MIT transition in k-TP thin films comes from the electron interaction, which can be controlled by modifying the lattice parameters or the chemical composition while essentially maintaining the original lattice structure. The application of hydrostatic pressure is an effective way to change the intermolecular distance and hence change the electronic interaction. As shown in Figs. 4f, S8a and S8b, the increasing pressure reduces the electrical conductivity for k-TP thin film. The electrical resistivity change is defined as $(R_{P=1\ Pa}-R_{P=200\ kPa})/(R_{P=200\ kPa})$, where $R_{P=1\ Pa}$ and $R_{P=200\ kPa}$ represent the electrical resistivity of k-TP thin film at 1 Pa and at 200 kPa, respectively. The obtained electrical resistivity changes in the

first cycle are -11 □, -33 □ and -12 □ for T=300 K, 135 K and 126 K, respectively. A pressure cycling (up to 50 cycles) test of electrical resistivity is performed on the k-TP thin film. Figure 4d shows electrical resistivity of the sample for the 50 cycles at T=135 K. It is clearly shown that the electrical resistivity does not show a significant decrease with increasing cycle numbers, suggesting its good stability. The pronounced pressure effect in the MIT transition

region is resulted from a metastable state where metallic and insulating state co-existent in k- TP thin film. Theoretical calculation is performed to study the mechanism of pressure reduced electrical conductivity. Figure 4e presents the pressure dependence on DOS of k-TP. We can observe a decrease of electronic states at Fermi level with increasing pressure, from 7.2 states/ev at 0 GPa to 5.9 states/eV at 0.5 GPa (Figure 4f). The result indicates that the pressure leads to the metallicity weakening of k-TP. Additionally, we build a slab model of k-TP along
[010] directions with the setting the vacuum as 15 Å. We find that the electronic states at Fermi level reach to 16.05 states/eV for the same number of atoms as unit cell, which implies a strengthening of metallicity.

The light illumination effect on the electrical properties of k-TP is shown in **Figure 5**a, where no light effect is shown in both metallic and insulating states. At the conducting state, the charge carrier density is high in k-TP, while the band gap at the insulating state is too large for the visible light to excite the electrons from valence to conduction band. However, a pronounced light effect is shown in the MIT transition region, at which the light-induced electrical resistivity is decreased by 50%. During the MIT transition, the bandgap increases continuously as decreasing temperature. At the MIT region, the bandgap reaches the same energy level as the photon energy of visible light, and thus more charge carriers are generated under light illumination for photoconductivity (Figure 5b).

Conclusion

There has been considerable interest in strongly correlated electronic molecules. Our results present that molecular conducting and plasmonic k-

TP thin film shows a strong electron correlation and coupling between charge, spin and lattice degrees of freedom. Accompanied with the metal-to-insulator transition, the simultaneous transition occurs from paramagnetic, electrical and thermal conducting state to diamagnetic, electrical and thermal insulating state. The density functional theory calculation and spectroscopy studies provide the mechanistic

understanding of electron correlation and molecular plasmon resonance observed in molecular conducting film

(1)

Experimental Section

As shown in Figure 1a, the k-PT thin films were prepared by sealing the pure potassium lumps, p-terphenyl and glass substrate together inside the high-vacuum glass tube. Then the glass tube was annealed at different sintering temperature for two days to deposit k-PT thin film on the glass substrate with pre-patented 50 nm sliver electrode deposited using a high vacuum electron beam evaporation system (Kurt J Lesker, AXXIS). The electrode distance is 50 μm. The samples were selaed with polydimethylsiloxane in the glovebox for the electrical and optical measurements. I-V characteristics were measured using an interfaced Keithley 2400 by four probe method. Temperature dependence of resistance measurements were carried out by four probe method with a Keithley 2400 constant current source. X-ray powder diffraction pattern was obtained with a RIGAKU Ultima-IV diffractometer and intensity data were collected at steps of 0.02° (Cu, Kα). Raman microspectroscopy was performed using a RenishawinVia. Raman microscope (Renishaw, Inc. Hoffman Estates, IL), equipped with a Leica DMLM microscope (5×, 20× and L50×objectives). Spectra were collected using a Renishaw diode laser (514 nm, ~2 μm × 20 μm irradiated area, 1260 lines/mm grating). The microstructure examination was performed in a field emission gun

scanning electron microscope (JSM 7001F, Jeol). The magnetic and thermal conductive properties were studied by a Physical Property Measurement System (PPMS) of Quantum Design company. Optical absorbance spectra were obtained with an Agilent Cary 7000 Universal Measurement

Spectrophotometer. The XAS measurement was performed using Beamline 6.3.1.1 at the 174 Advanced Light Source (Berkeley, CA).

Within the framework of density functional theory, the Vienna *ab* initio simulation package based on the projector augmented wave method was employed to optimize lattice parameters and calculate the electronic structures.[28, 29] The generalized gradient approximation of the exchange-correlation functional (Perdew-Burke-Ernzerh of 96, PBE) was adopted.[30] Considering the non-local interactions, we added the correction of van der Waals (vdW) in the version of vdW-DF2 in the calculations.[31] The adopted energy cutoff 600 eV. Structural optimization used a conjugate-gradient algorithm and the *k*-point of the Brillouin zone is 0.04 $Å^{-1}$ interval distribution of Monkhorst-Pack. The *k*-point interval of the total energy selfconsistent calculation is 0.02 $Å^{-1}$. The convergence criterion of force is 10^{-3} eV/Å. The energy convergence standard is 10^{-6} eV.

Supporting Information

Supporting Information is available from the Wiley Online Library or from the author.

Acknowledgements

Y.H., G.H.Z., Y.-S.G., and J.N.A. contributed equally to this work. The U.S. Department of Energy, Office of Basic Energy Sciences, Division of Materials Sciences and Engineering supports S.R. under Award DE-

SC0018631 (Organic conductors). Financial support was provided by the U.S. Army Research Office supports S.R. under Award. W911NF-18-2-0202 (Materials-by-Design and Molecular Assembly). C.L. and A.B. carried out thermal conductivity measurements, and were supported by the US Department of Energy, Office of

Science, Basic Energy Sciences, Materials Sciences and Engineering Division. The use of facilities at the Center for Nanoscale Materials, an Office of Science user facility was supported by the US Department of Energy, Basic Energy Sciences under Contract No. DE- AC02-06CH11357.

References

[1]. M. Imada, A. Fujimori, Y. Tokura, *Rev. Mod. Phys.* **1998,** *70*, 1039.

[2]. M. Uehara, S. Mori, C. Chen, S.-W. Cheong, *Nature* **1999,** *399*, 560.

[3]. E. Dagotto, *Rev. Mod. Phys.* **1994,** *66*, 763.

[4]. M. Liu, H. Y. Hwang, H. Tao, A. C. Strikwerda, K. Fan, G. R. Keiser, A. J. Sternbach,

K. G. West, S. Kittiwatanakul, J. Lu, *Nature*

2012, *487*, 345. [5]. A. Ramirez, *J. Phys.:*

Condens. Matter **1997,** *9*, 8171.

[6]. M. N. Wilson, Superconducting magnets. (Clarendon, Oxford, **1983**).

[7]. Z. Yang, C. Ko, S. Ramanathan, *Annu. Rev. Mater. Res.*

2011, *41*, 337-367. [8]. B. Radisavljevic, A. Kis, *Nat. Mater.*

2013, *12*, 815.

[9]. J. H. Park, J. M. Coy, T. S. Kasirga, C. Huang, Z. Fei, S. Hunter, D. H. Cobden,

Nature **2013,** *500*, 431.

[10]. M. Fiebig, K. Miyano, Y. Tomioka, Y. Tokura, *Science* **1998,** *280*, 1925-1928.

[11]. Y. Joo, V. Agarkar, S. H. Sung, B. M. Savoie, B. W. Boudouris, *Science*

2018, *359*, 1391-1395.

[12]. J. R. Kirtley, J. Mannhart, *Nat. Mater.* **2008,** *7*, 520.

[13]. R. Mitsuhashi, Y. Suzuki, Y. Yamanari, H. Mitamura, T. Kambe, N.

Ikeda, H. Okamoto, A. Fujiwara, M. Yamaji, N. Kawasaki, *Nature* **2010,**

464, 76.

[14]. H. Sirringhaus, P. Brown, R. Friend, M. M. Nielsen, K. Bechgaard, B. Langeveld- Voss, A. Spiering, R. A. Janssen, E. Meijer, P. Herwig, *Nature* **1999,** *401*, 685.

[15]. H. Alves, A. S. Molinari, H. Xie, A. F. Morpurgo, *Nat. Mater.* **2008,** *7*, 574.

[16]. J. L. Bredas, G. B. Street, *Acc. Chem. Res.* **1985,** *18*, 309-315.

[17]. J. M. Luther, P. K. Jain, T. Ewers, A. P. Alivisatos, *Nat. Mater.* **2011,** *10*, 361. [18]. M. Dressel, N. Drichko, *Chemical reviews* **2004,** *104*, 5689-5716.

[19]. R. Haddon, A. Hebard, M. Rosseinsky, D. Murphy, S. Duclos, K. Lyons, B. Miller, J. Rosamilia, R. Fleming, A. Kortan, *Nature* **1991,** *350*, 320.

[20]. Y. Hu, G. H. Zhong, Y.-S. Guan, N. H. Lee, Y. Zhang, Y. Li, T. Mitchell, J. N. Armstrong, J. Benedict, S. W. Hla, S. Q. Ren, *Adv. Mater.* **2019,** 1807178.

[21]. Y. Furukawa, H. Ohtsuka, M. Tasumi, *Synth. Met.* **1993,** *55*, 516-523.

[22]. A. A. da Costa, N. Karger, A. Amado, M. Becucci, *Solid State Ionics* **1997,** *97*, 115- 121.

[23]. R. Snyder, S. Hsu, S. Krimm, *Spectrochim. Acta, Part A* **1978,** *34*, 395-406.

[24]. N. Hassan, S. Cunningham, M. Mourigal, E. I. Zhilyaeva, S. A. Torunova, R. N. Lyubovskaya, J. A. Schlueter, N. Drichko, *Science* **2018,** *360*, 1101-1104.

[25]. H. Matsuzaki, W. Fujita, K. Awaga, H. Okamoto, *Phy. Rev. Lett.* **2003,** *91*, 017403. [26]. D. Jérome, **1991,** *252*, 1509-1514.

[27]. T. Sugimoto, H. Fujiwara, S. Noguchi, K. Murata, *Sci. Technol. Adv. Mater* **2009,** *10*, 024302.

[28]. G. Kresse, J. Furthmüller, *Comput. Mater. Sci.* **1996,** *6*, 15-50.

[29]. J. P. Perdew, A. Zunger, *Phys. Rev. B* **1981,** *23*, 5048.

[30]. J. P. Perdew, K. Burke, M. Ernzerhof, *Phys. Rev. Lett*. **1996,** *77*, 3865.

[31]. K. Lee, É. D. Murray, L. Kong, B. I. Lundqvist, D. C. Langreth, *Phys. Rev. B* **2010,** *82*, 081101.

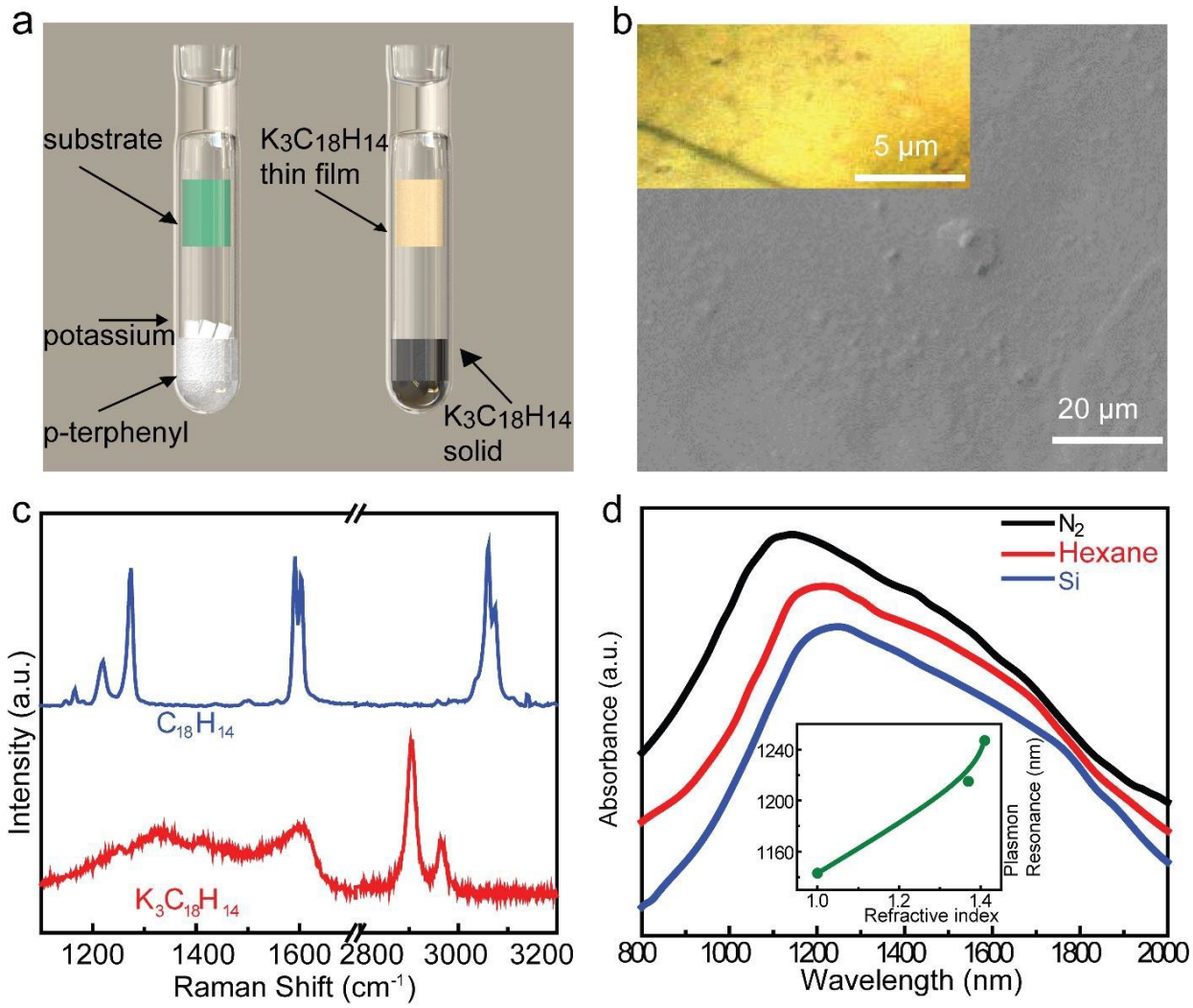

Figure 1. Structural and electrical characterization of k-TP thin films ($K_3C_{18}H_{14}$ prepared at 573 K). a) Schematic growth diagram of potassium-doped p-terphenyl thin film. b) Scanning electron microscopy images of k-TP thin film, respectively. Inset shows the optical image of k-TP thin film. c) Raman spectra of k-TP thin film and pristine p-terphenyl samples. d) Absorbance for k-TP thin film at different environment. Inset shows the reflect index dependence of plasmon resonance frequency.

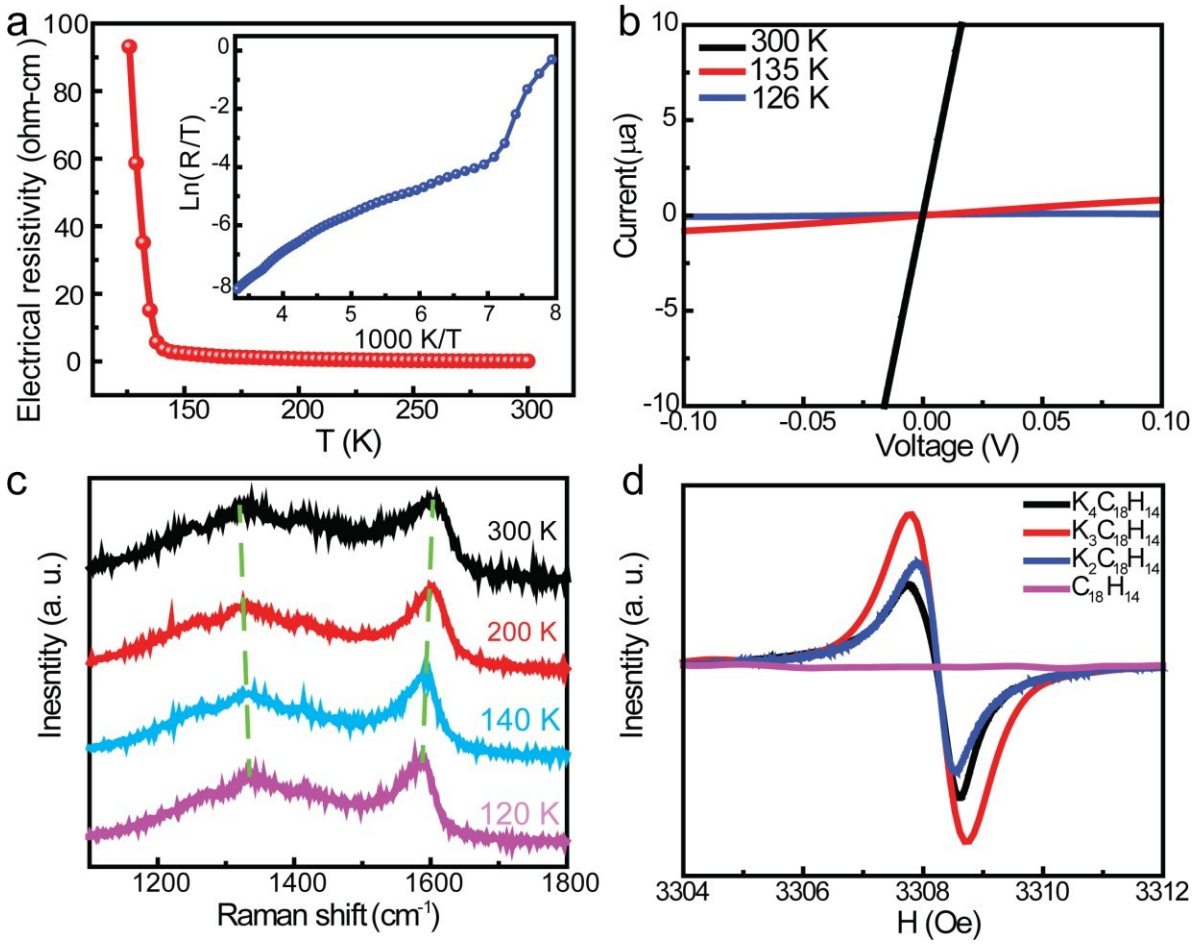

Figure 2. Electrical, Raman and EPR characterization of k-TP thin film prepared at 573 K. a) Temperature dependence of electrical resistivity of k-TP thin film. Inset shows the logarithm of electrical resistivity(R)/temperature vs. the inverse temperature for k-TP thin film. b)I-V curves for k-TP thin film at different temperature. c) Raman of k-TP thin film and pristine p- terphenyl at different temperature. d) EPR of $K_xC_{18}H_{14}$ thin film and pristine p-terphenyl.

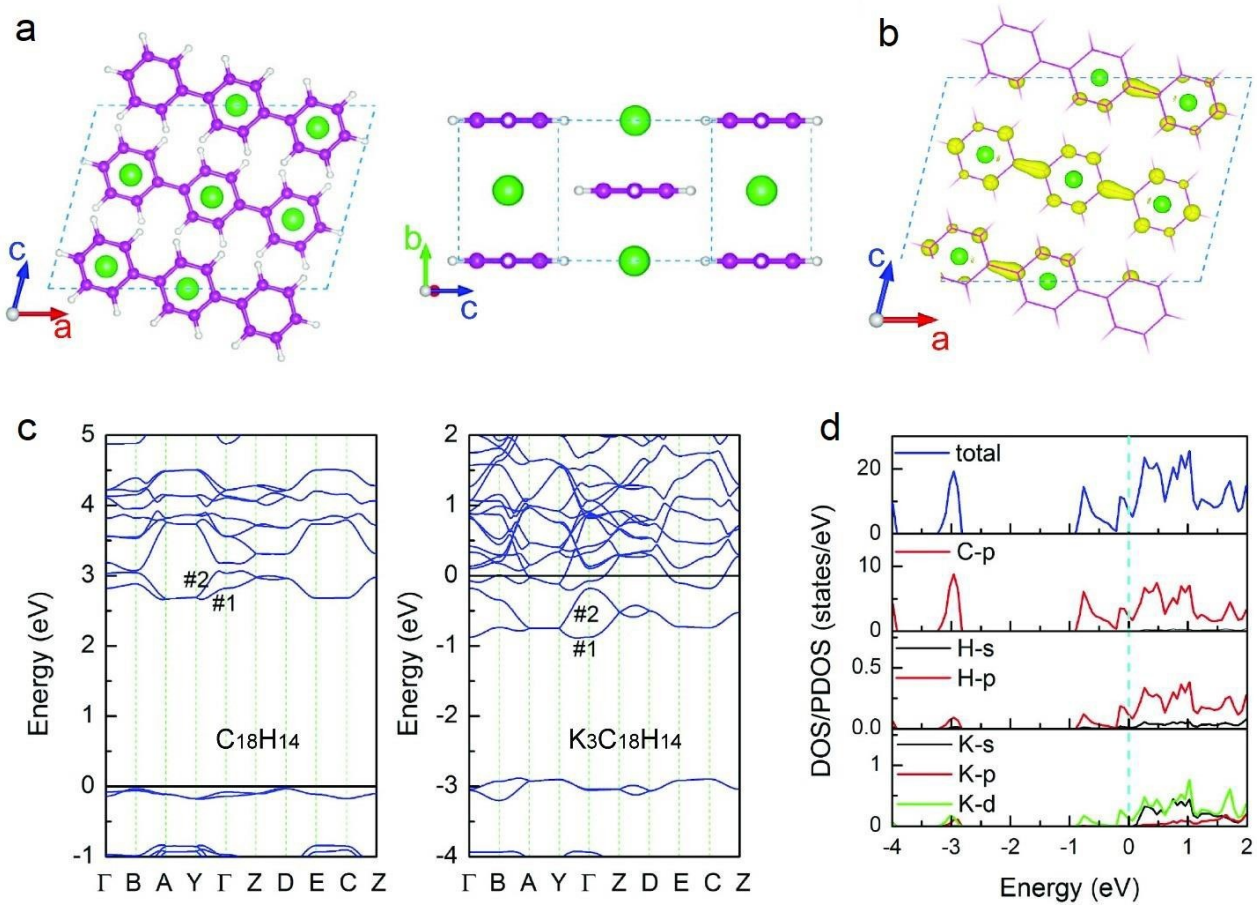

Figure 3. Theoretical calculation of the metallic behavior in k-TP. a) Optimized structures of k-TP viewing from different directions. b) Calculated 3D plots of different charge density for k-TP with the isosurface unit of 4×10^{-3} e/a.u.^{3}. Pink, white, and green balls represent C, H, and K atoms, respectively. The yellow and light blue areas mean the increase and the decrease of electrons in this region, respectively. c) Band structure for pristine p-terphenyl and k-TP. Zero energy denotes the Fermi level. d) Electronic DOS for pristine p-terphenyl and k-TP. Zero energy denotes the Fermi level.

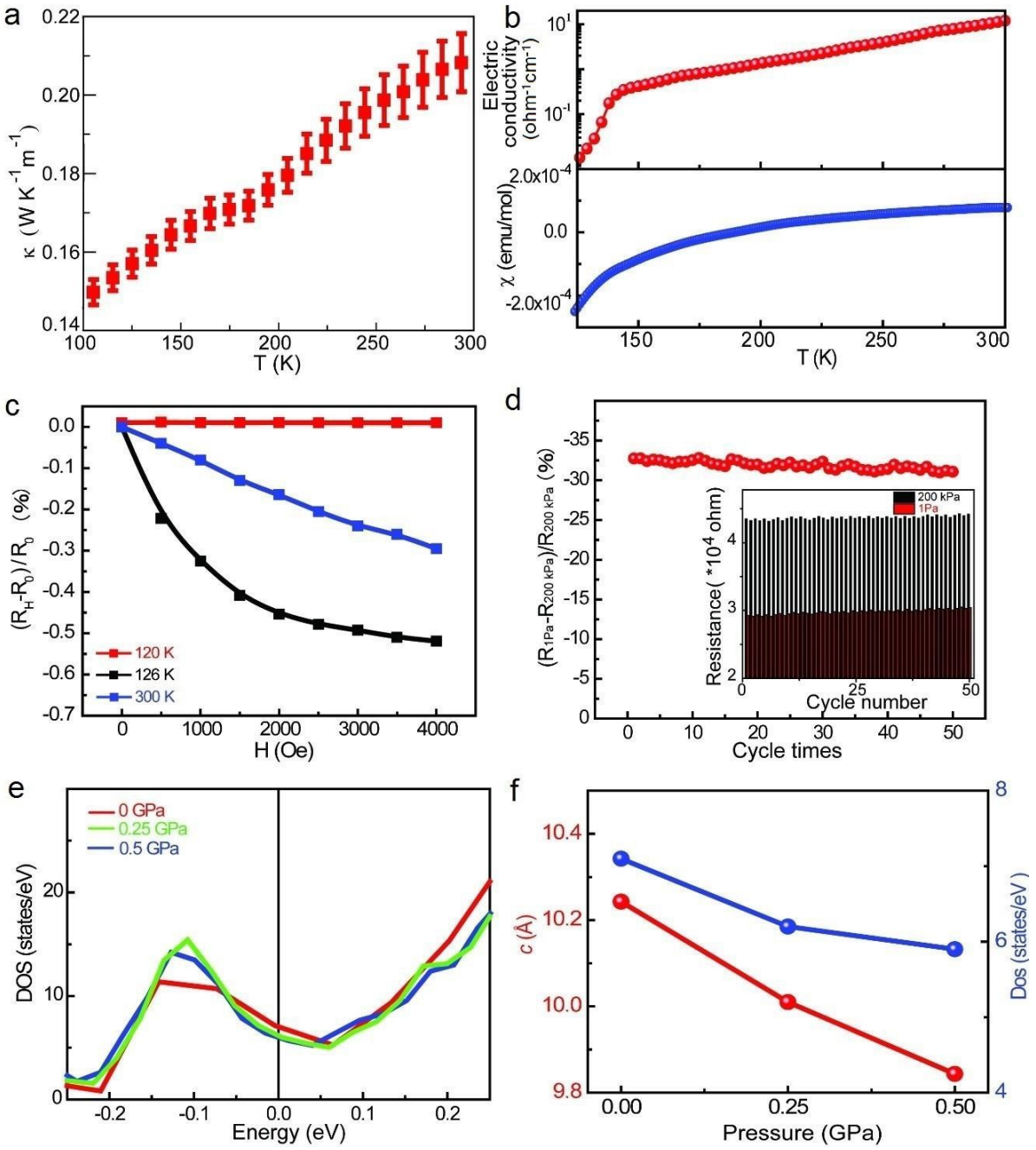

Figure 4. Charactering the coupling between charge, spin, and lattice degrees of freedom for k-TP sample prepared at 573 K. a) Temperature dependence of thermal conductivity for k-TP sample. b) Temperature dependence of electrical conductivity and magnetic susceptibility for $K_3C_{18}H_{14}$ thin film. c) Magnetoresistance for k-TP thin film at different temperature. d) Pressure induced resistivity change for k-TP sample at 135 K. Inset shows the stability test up to 50 cycles. e) Pressure dependence

on DOS. f) Pressure dependence of lattice parameter for *c* axis.

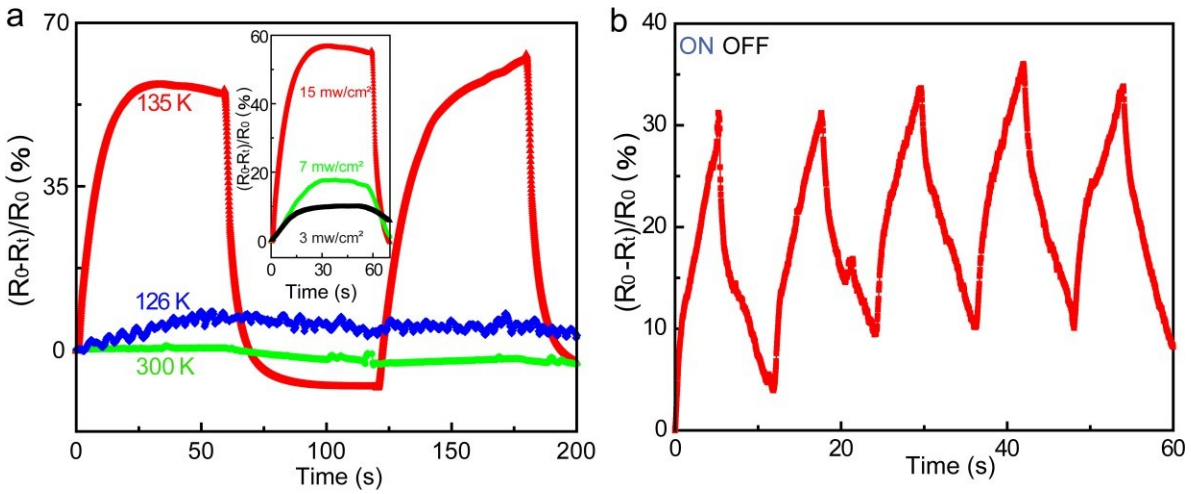

Figure 5. Light effect for k-TP thin film prepared at 573 K. a) The photoresponse and the on- off ratio of k-TP different temperature under solar illumination 15 mw/cm^2 at 2 V. Inset shows the photoresponse and the on-off ratio of k-TP at 135 K under solar illumination with different light intensity at 2 V. b) Stability test for the photoresponse of k-TP at 135 K under solar illumination 15 mw/cm^2 at 2 V.

Table of contents

Self-assembled molecular plasmonic films are prepared. The coupling of charge, spin, lattice, and orbital degrees of freedom enables the switchable metal-to-insulator transition under external stimuli, at which the simultaneous transition occurs from paramagnetic, electrical and thermal conducting state to diamagnetic, electrical and thermal insulating state **Keyword**

charge-transfer, molecular conductor, aromatic molecule, surface plasmon resonance

Yong Hu, Guohua Zhong, Ying-Shi Guan, Jason N. Armstrong, Changning Li, Changjiang Liu, Alpha N'Diaye, Anand Bhattacharya, and Shenqiang Ren*

Strongly Correlated Aromatic Molecular Conductor

ToC figure

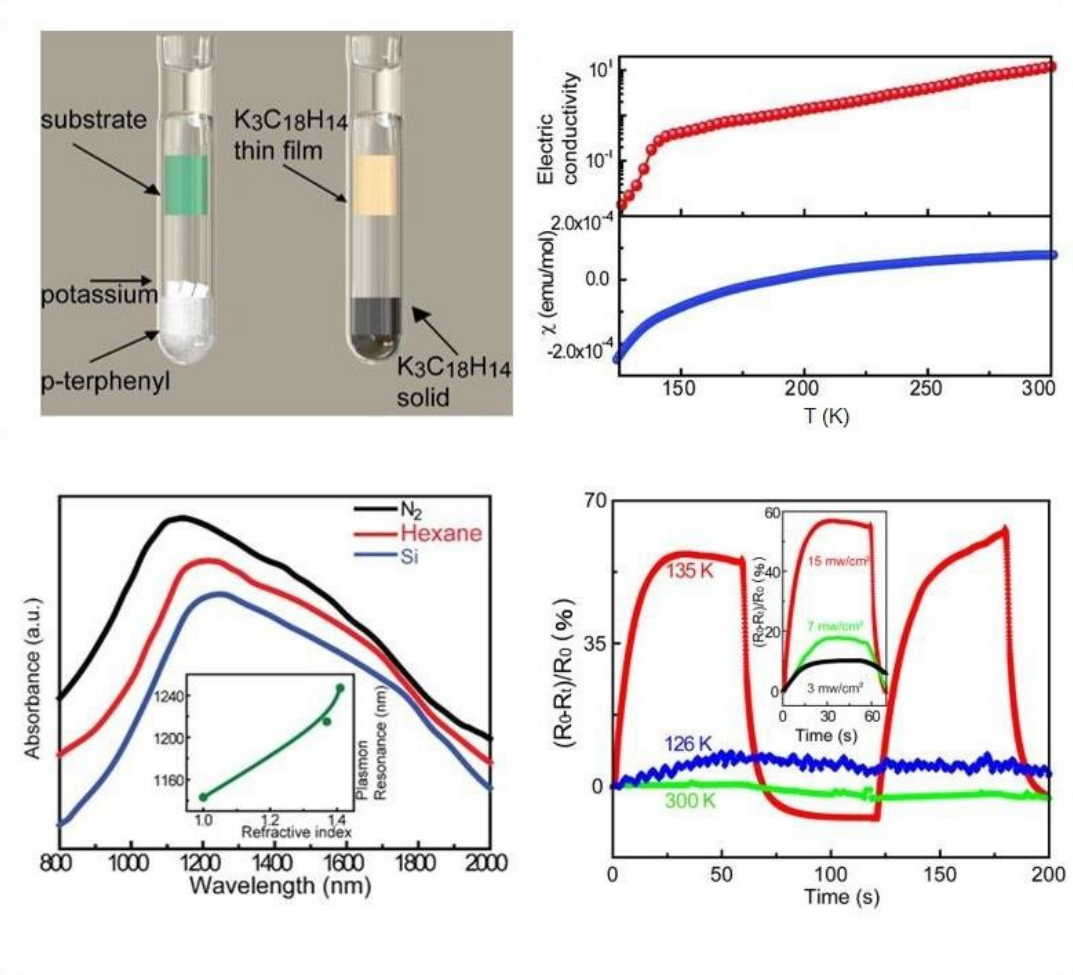

Supporting Information

Strongly Correlated Aromatic Molecular Conductor

*Yong Hu, Guohua Zhong, Ying-Shi Guan, Jason N. Armstrong, Changning Li, Changjiang Liu, Alpha N'Diaye, Anand Bhattacharya, and Shenqiang Ren**

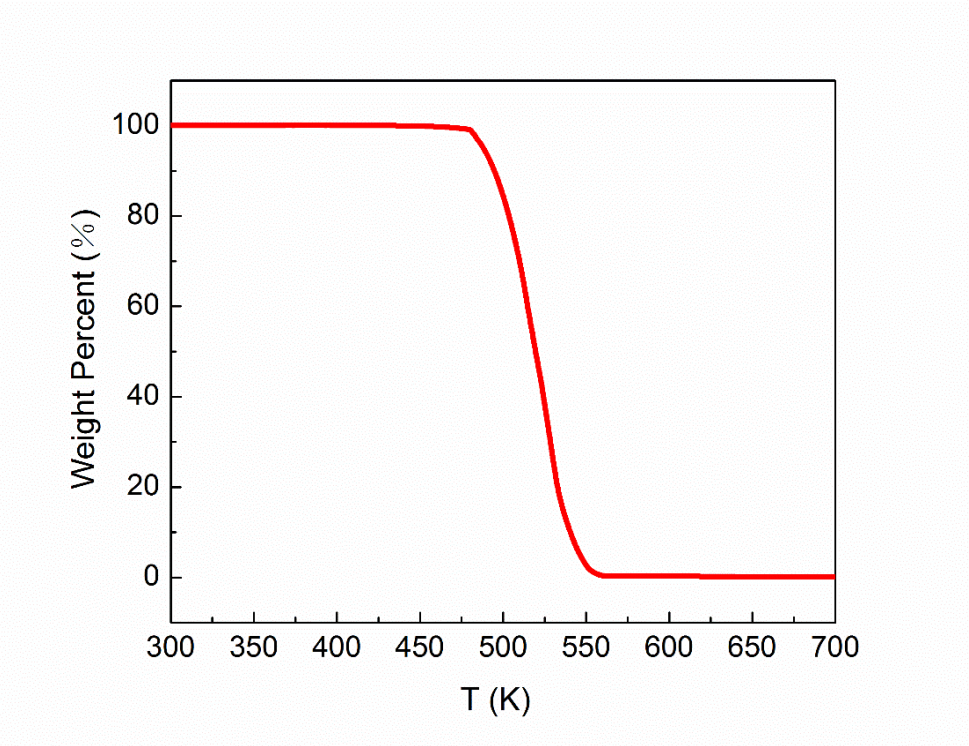

Figure S1. TGA for pristine p-terphenyl sample.

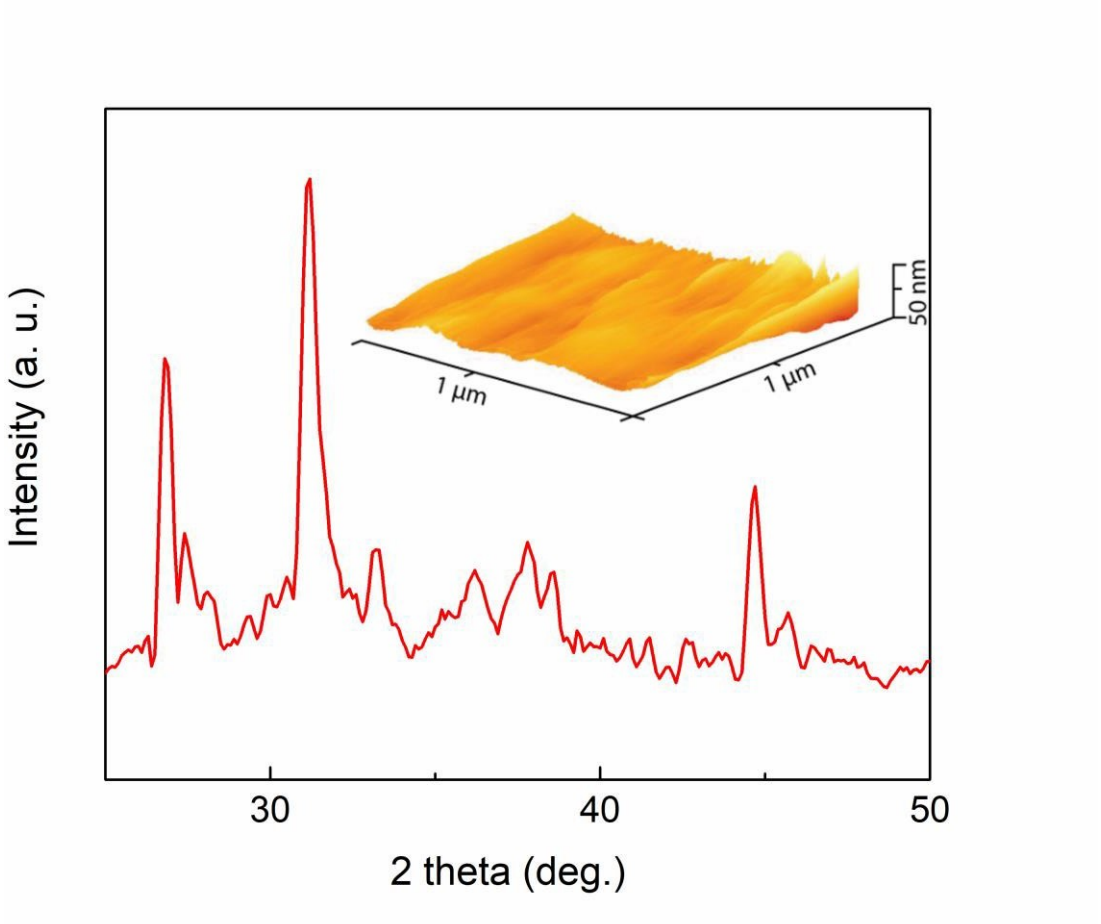

Figure S2. XRD pattern of $K_3C_{18}H_{14}$ powder, inset shows the AFM image of $K_3C_{18}H_{14}$ film.

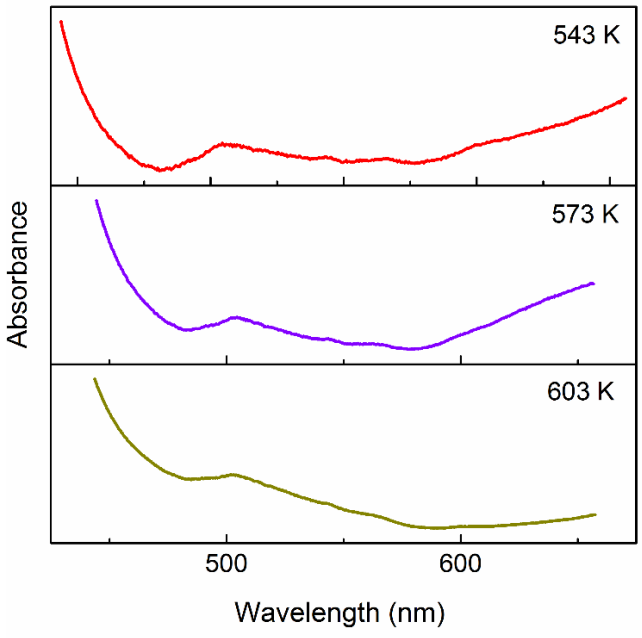

Figure S3. Absorbance spectra for $K_3C_{18}H_{14}$ sintered at 543, 573 and 603 K.

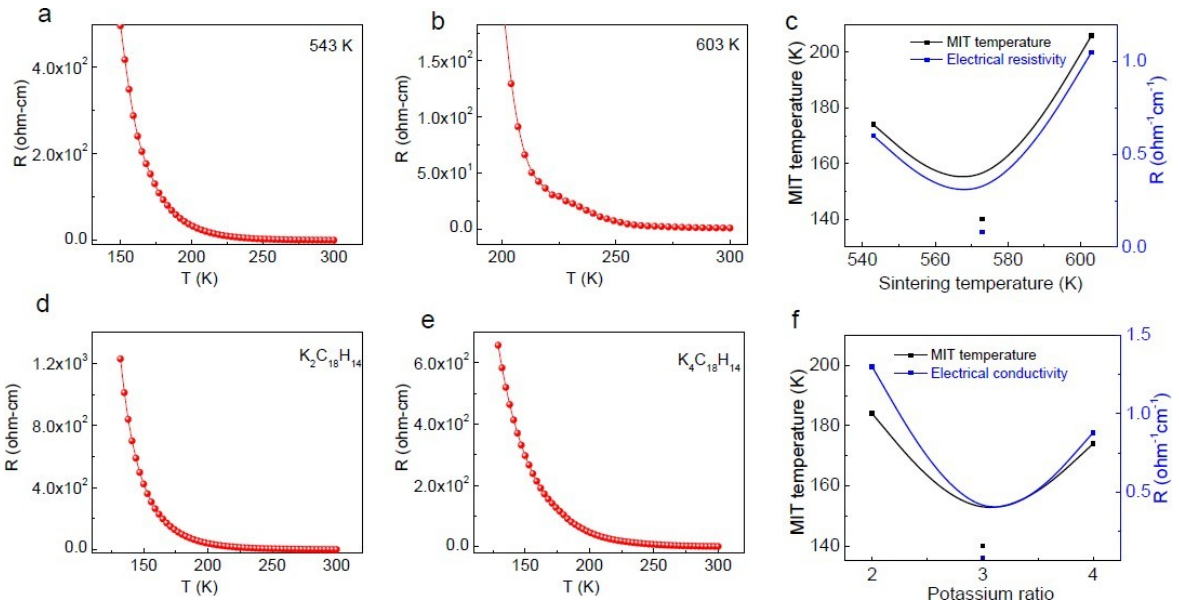

Figure S4. a, b, temperature dependence of electrical resistivity(R) in $K_3C_{18}H_{14}$ thin films for the thin film prepared at 543 K and 603 K, respectively. c, Sintering temperature dependence of MIT temperature and electrical resistivity (300K) obtained from the temperature dependence of electrical resistivity curves. d, e, Temperature dependence of electrical resistivity of $K_2C_{18}H_{14}$ and $K_4C_{18}H_{14}$, respectively. f, Potassium doping ratio dependence of MIT temperature and electrical resistivity (300K) obtained from the temperature dependence of electrical resistivity curves.

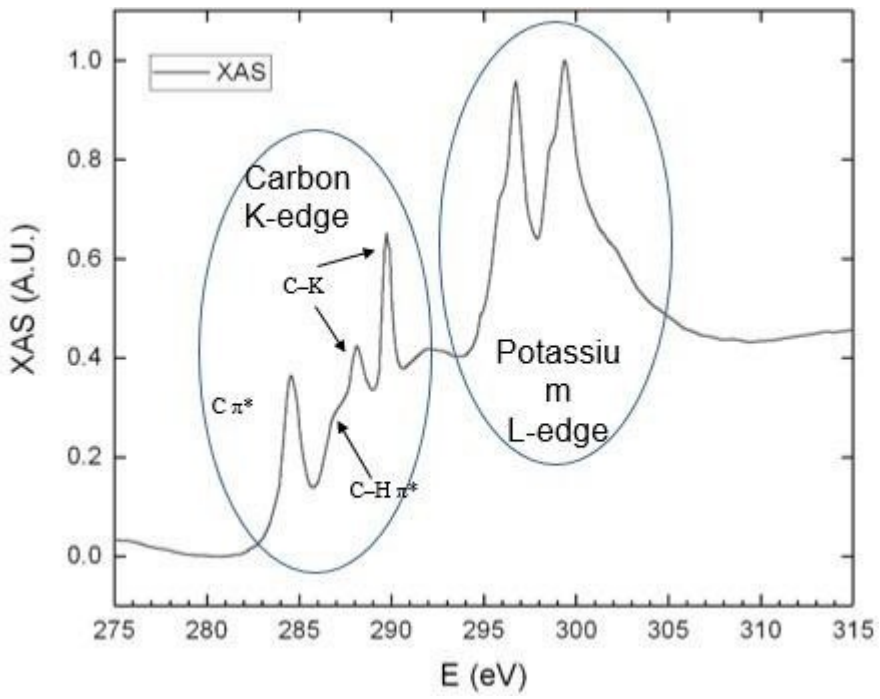

Figure S5. X-ray absorption spectroscopy for $K_3C_{18}H_{14}$ prepared at 603 K.

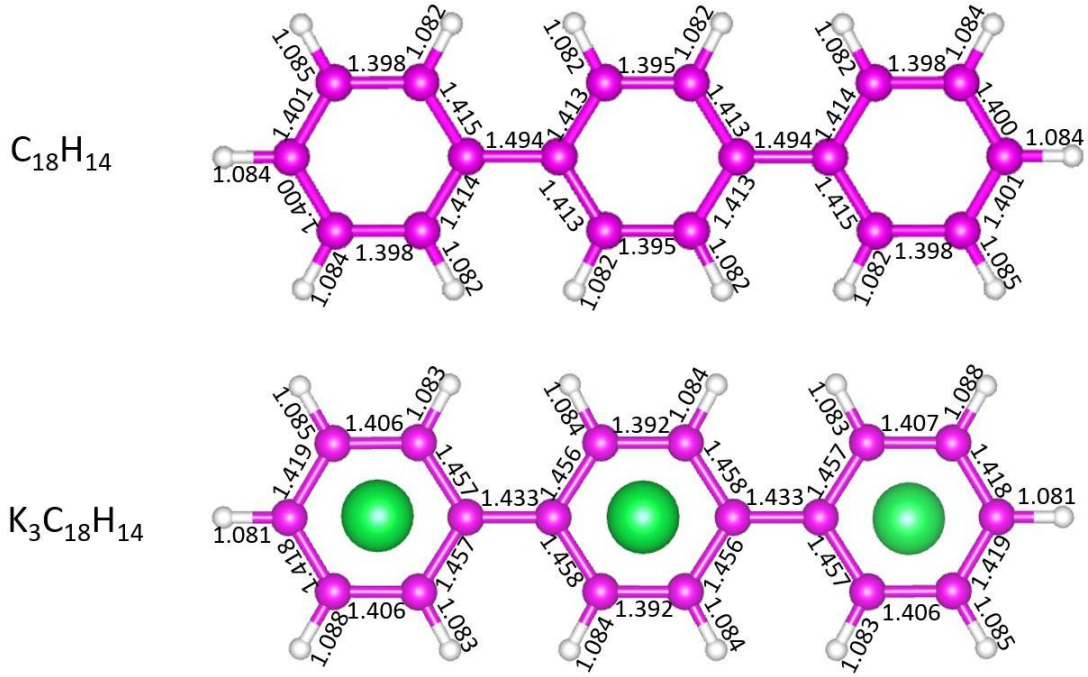

Figure S6. Calculated bond length for $C_{18}H_{14}$ and $K_3C_{18}H_{14}$.

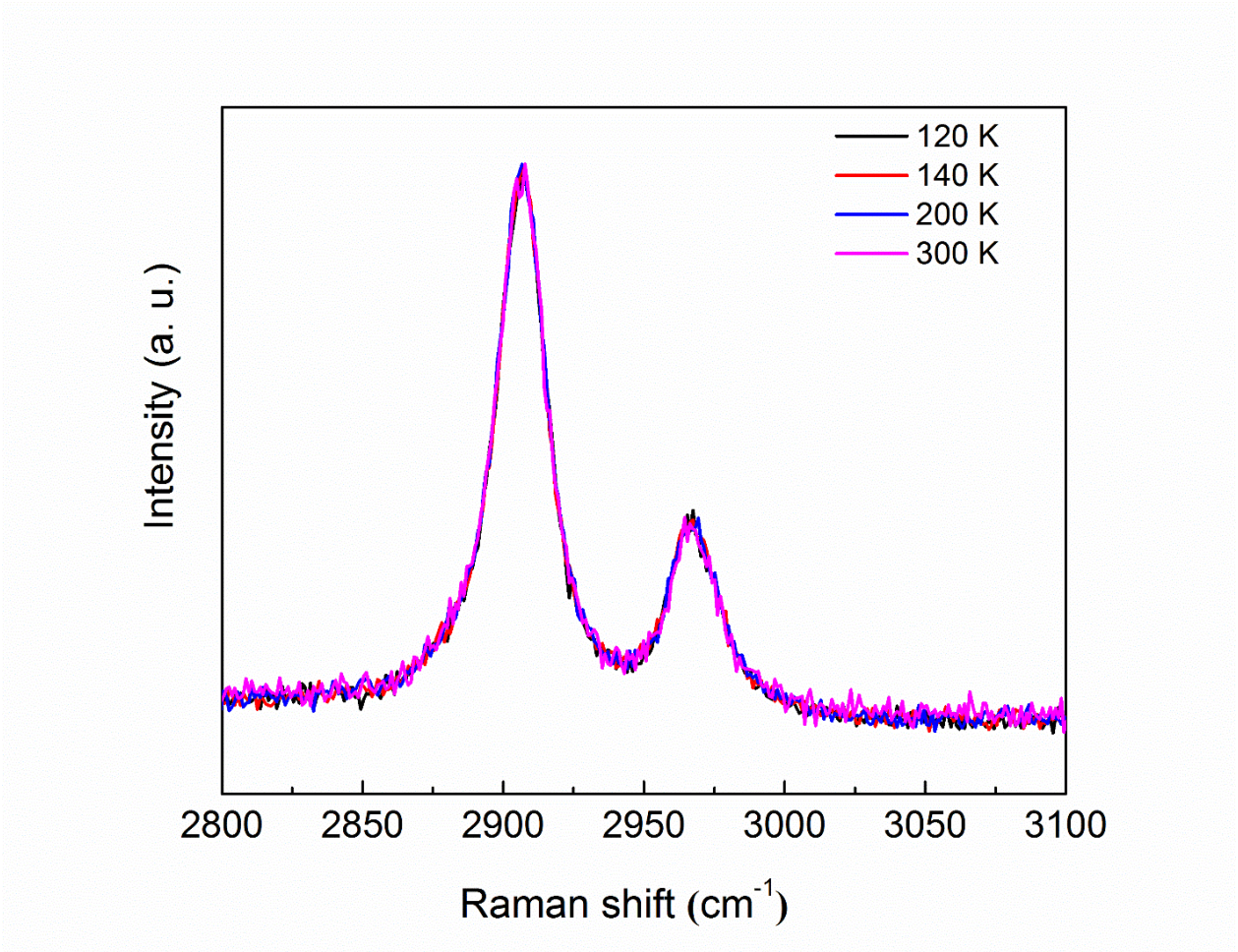

Figure S7. Raman spectra for $K_3C_{18}H_{14}$ thin film.

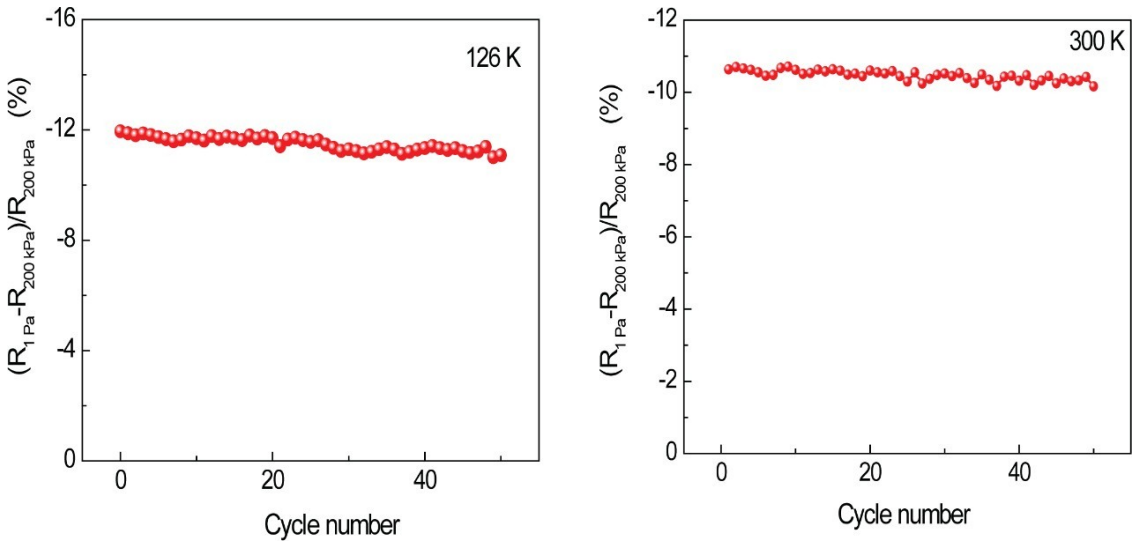

Figure S8. a, b, Pressure induced electrical resistivity(R) change for $K_3C_{18}H_{14}$ sample at 126 K and 300 K.